Cement and Concrete Research 132 (2020) 106051

Contents lists available at ScienceDirect

Cement and Concrete Research

journal homepage: www.elsevier.com/locate/cemconres

Reinforcement corrosion in limestone flash calcined clay cement-based concrete

Quang Dieu Nguyen[a,*,1], Arnaud Castel[b]

[a] Centre for Infrastructure Engineering and Safety, School of Civil and Environmental Engineering, The University of New South Wales, Sydney, NSW 2052, Australia
[b] School of Civil and Environmental Engineering, The University of Technology Sydney (UTS), Sydney, NSW 2007, Australia

ARTICLE INFO

Keywords:
LC3
Flash calcined clay
Limestone
Low-carbon concrete
Durability
Corrosion

ABSTRACT

Limestone calcined clay cement (LC3) concrete has attracted world-wide attention as a newly promising low-carbon concrete. In this study, long-term reinforcement corrosion in LC3 concrete was investigated. Both chloride and carbonation-induced reinforcing bar corrosion were examined. Open circuit corrosion potential, polarization resistance, Tafel constants were monitored at regular intervals up to 500 days. Gravimetric mass loss was measured and compared to the loss of mass calculated using electrochemical methods. The performance of concrete with flash calcined clay and limestone was similar to that of traditional Portland cement concrete in long-term investigation. Traditional corrosion methods and classifications used widely to assess of steel in concrete can be applied to concrete containing LC3 providing a recalibration of polarization resistance range for passitivity condition.

1. Introduction

Reinforcement corrosion in concrete structures is one of the most challenging issues in both developed and developing countries. Corrosion-related deterioration direct cost was considered more significant than expenditure spent on medical problems such as obesity and cigarette smoking or natural disasters [1–5]. In addition, the continual ageing and degradation of current reinforced concrete structures escalate the financial burden on maintenance, rehabilitation or even replacement of deteriorated infrastructure [6]. The corrosion process can be divided into two stages based on a well-known schematic proposed by Tuutti: initiation stage and propagation stage [7]. In the first stage, aggressive agents including chloride ions or carbon dioxide diffuse through the concrete porosity toward the steel-concrete interface until the conditions of reinforcing bars depassivitation are fulfilled (critical chloride threshold or acidification of passive film to pH value < 9). When reinforcement is depassivitated, the propagation stage starts with the formation and accumulation of corrosion products together with rebar cross-section reduction and cracking/spalling of concrete. Although the ingress of chloride ion or CO_2 to trigger reinforcement corrosion in initiation stage was relatively well-documented, many questions in propagation stage have been remained unsolved due to complex electrochemical redox process involving both chemical reactions and electrical current exchanges [1,8,9].

Supplementary cementitious materials (SCMs) have been utilized as ordinary Portland cement (OPC) substitution in construction industry for several decades to reduce the carbon dioxide emission in cement production and their utilization has been in increasing demand to fulfil the target of decarbonation by 2050 [10]. Due to the limited quantities of traditional SCM such as fly ash and slag on global scale, calcined clay and limestone have been presented as a potential alternative based on their substantially worldwide availability [11]. Previous studies reported the synergetic effect of calcined clay and limestone as binder replacement to form AFm phases in order to compensate early strength reduction by other SCM [12–14]. Flash calcined clay manufactured by flash calcination in the duration of a few tenths of a second can diminish up to 80% the energy required for Portland cement production [15,16]. Therefore, a combination of flash calcined clay and limestone can provide a remarkable contribution to minimize the anthropogenic CO_2 emissions. The durability properties during initial phase of corrosion in Portland cement, calcined clay and limestone concrete were studied in terms of chloride and carbonation diffusion resistance. An excellent performance in term of chloride diffusion resistance was attributed to refinement of pore structures and chloride binding capacity whereas low resistance toward CO_2 penetration was reported [13,17–21]. Conventional standard testing methods for durability were evaluated to compare the performance of calcined clay limestone blended concrete, traditional plain OPC and fly ash blended concrete

* Corresponding author.
E-mail addresses: qd.nguyen@unsw.edu.au, quangdieu.nguyen@uts.edu.au (Q.D. Nguyen).
[1] Current address: School of Civil and Environmental Engineering, The University of Technology Sydney (UTS), Sydney, NSW 2007, Australia.

https://doi.org/10.1016/j.cemconres.2020.106051
Received 3 September 2019; Received in revised form 17 February 2020; Accepted 22 March 2020
Available online 31 March 2020
0008-8846/

such as rapid chloride penetration test, concrete resistivity, gas permeability, water sorptivity etc. [22–24]. The influence of limestone and calcined clay on chloride diffusion coefficient, ageing coefficient and chloride threshold was integrated into probabilistic service life models showing that LC3 concrete can achieve a longer service life in chloride environments [25]. Due to limited literature about long-term performance of flash calcined clay limestone cement concrete toward reinforcement corrosion, this study aims to investigate the corrosion process in propagation stage of reinforced LC3 concrete. The initiation phase was accelerated for both chloride and CO_2 penetration but propagation phase remained in natural condition. Open circuit corrosion potential, polarization resistance, Tafel constants were monitored up to 500 days of corrosion propagation. The performance of LC3 concrete was compared with OPC conventional concrete to reveal the impact of flash calcined clay and limestone on concrete performance. The suitability of current corrosion classifications to be used for LC3 concrete was assessed. Gravimetric mass loss measurements were carried out to validate the electrochemical experiment specifications.

2. Materials and methodology

2.1. Materials and mix compositions

Ternary combination of General Purpose (GP) cement, flash calcined clay and limestone was used to fabricate LC3 concrete. OPC constitutes about 90 wt% of GP cement and 7 wt% to 8 wt% of mineral additions with 2 wt% to 3 wt% of gypsum are allowed in GP cement. Calcined clay is produced by flash calcination process from Argeco, France and limestone is branded as Stonedust supplied by Boral Limited, Australia. The amorphous content of flash calcined clay is 50.9 wt% reported in previous study of authors, which is defined as low-grade calcined clay [24]. Chemical compositions of binder determined by X-ray fluorescence (XRF) and mineralogical compositions of GP cement and flash calcined clay analysed by XRD-Rietveld are presented in Table 1. Sydney sand and 10 mm nominal size Basalt were utilized as fine and coarse aggregate with the specific gravities of 2.65 and 2.8 respectively. To achieve a concrete compressive strength of about 45 MPa, which is a minimum standard requirement in chloride environment, 20 wt% of GP cement was substituted by a combination of flash calcined clay and limestone with a ratio of 2:1 by mass. The reason why no > 20 wt% replacement could be achieved is that the flash calcined clay used was coarser than calcined clays used in other studies where 50 wt% replacement was achieved [12,24,26]. Moreover, the kaolinite of the raw clay was 55 wt%, which is defined as low-grade calcined clay [27]. However, using lower grade clay provides advantages in blended cements as higher-grade clay diminishes the long-term hydration of clinker phases leading to the inefficient clinker utilization in low clinker cements [28]. In addition, the proportion of OPC in the mix design approximately 72 wt% due to actual percentage of OPC in GP cement as mentioned in the beginning of this section. The same mix design was used for the accelerated carbonation test. Table 2 shows mix proportioning with all aggregate in saturated surface dry (SSD) condition. All aggregates were over-dried at 105 °C for at least 24 h to remove any moisture remaining, then cooled down and added calculated SSD water amount prior to concrete casting.

Table 1
Chemical composition and mineralogical composition of binder.

	GP cement (wt %)	Calcined clay (wt %)	Limestone (wt%)
Chemical composition by XRF			
SiO_2	19.74	70.42	0.36
Al_2O_3	4.70	22.34	0.11
Fe_2O_3	2.98	2.34	0.1
CaO	64.62	0.49	57.51
MgO	1.48	0.16	0.29
Na_2O	0.21	0.1	–
K_2O	0.64	0.19	–
TiO_2	0.31	1.1	–
SO_3	2.24	0.02	–
Loss on ignition (LOI)	3.18	1.76	42.61
Mineralogical composition by XRD-Rietveld			
C_3S	51.2	–	–
C_2S	16.5	–	–
C_3A	6.5	–	–
C_4AF	7.3	–	–
Quartz	–	49.1	–
Amorphous	–	50.9	–

Table 2
Mix composition.

Materials (kg/m^3)	LC3
Coarse aggregate	1221
Fine aggregate	620.8
GP cement	310.4
Flash calcined clay	50.44
Limestone	27.16
Total binder (GP cement, flash calcined clay, limestone)	388
Water	174.5
Water/binder	0.45
Superplasticizer (wt%/binder)	0.61
Slump (mm)	120

2.2. Specimen specifications and exposure condition

A specific procedure was followed to assess the corrosion process in propagation phase, which was successful utilized in previous studies [29,30]. Fig. 1 presents the details of concrete specimen and embedded reinforcement. All rebars were 50 mm in length and 12 mm in diameter with 500 MPa yield strength. Reinforcing bars were cleaned using metal brush to remove all pre-existing rusts due to atmospheric corrosion and then weighted and labelled for gravimetric mass loss measurement at the end of the tests. Subsequently, the bars were stored in a vacuum desiccator at temperature of 23 °C to prevent any formation of rusts prior to the fabrication of the specimen. An electrical copper wire was brazed to one end of the reinforcing bar to facilitate the electrochemical measurements. To ensure a concrete cover of 15 mm from the exposure surface, both ends of bars were machined to fit the internal diameter of two polyvinyl chloride (PVC) tubes. Two holes were drilled in the mould to fit the two PVC tubes to maintain the 15 mm concrete cover during concrete casting. The tubes were also filled by silicon sealant to avoid the penetration of aggressive ions to the steel bars through the tubes. All reinforcing bars were placed in moulds one day prior to concrete casting to limit pre-rust formation which could affect the experimental mass loss assessment.

SSD aggregates, GP cement, flash calcined clay and limestone were dry-mixed about 5 min and then water was added and mixed for another 5 min. Eventually, fresh mixture filled the moulds by two layers and a vibrating table was employed for compacting each layer. Standard cylindrical specimens were also fabricated for testing of conventional mechanical, physical and durability properties. Moisture loss of fresh mixture was prevented utilizing appropriate lids. The specimens were demoulded after one day and placed in proper containers filled with water to mitigate the risk of excessive leaching issue during curing duration. In addition, top and bottom sides of corrosion samples were sealed with anti-corrosion foil to ensure the aggressive ions diffusion through only peripheral direction. After 7 days in water curing, the specimens were stored in a room with fixed temperature of 23 ± 2 °C and relative humidity (RH) of 50 ± 3% until 28 days.

As the scope of this study is monitoring reinforcement corrosion in propagation phase, the initiation stage was accelerated for both chloride and carbonation diffusion after 28 days of curing. For the

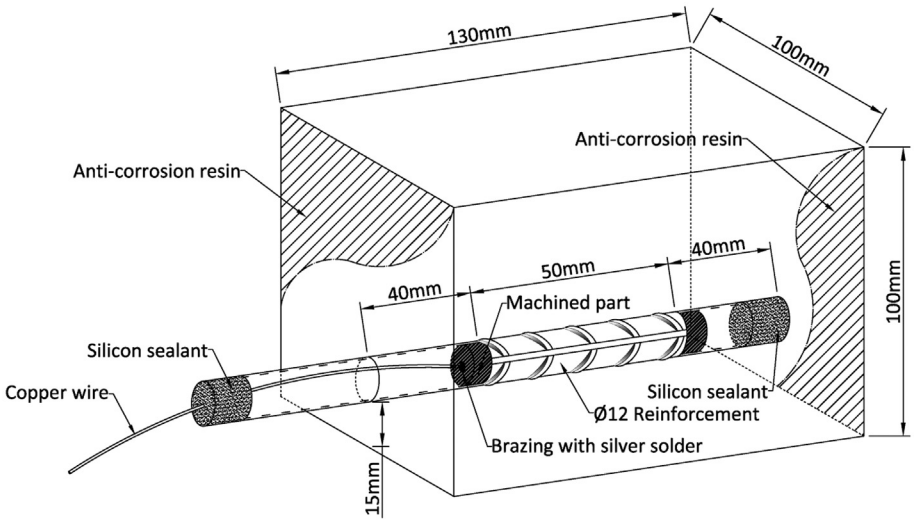

Fig. 1. Corrosion specimen specifications.

acceleration of chloride-induced corrosion, the specimens were oven-dried at 50 °C until constant mass to enhance their capillary capacity absorption of the chloride solution. Subsequently, they were rapidly submerged into sodium chloride solution with 35 g/l concentration, which is employed for previous plain cement concrete specimens [29]. Afterwards, alternate cycles of wetting and drying were conducted with the exposure condition of 1 week in sodium chloride solution (35 g/l concentration) and 2 weeks in air exposure at 23 ± 2 °C of temperature and 50% of RH. Regarding carbonation-induced reinforcement, specimens after 28 days of curing were placed in carbonation chamber with carbon dioxide concentration 1% with controlled temperature of 23 °C and RH of 55%. 1% CO_2 concentration leads to similar carbonation phases formation as observed in natural conditions with 0.03% CO_2 concentration according to XRD analysis [17,19,31]. Two series of specimens were used with different exposure periods to accelerate carbonation. For the first series, accelerated carbonation was stopped when the carbonation front reached the steel bar (see Section 2.4) and corrosion experiments then started. In terms of second series, specimens were stored for an additional six weeks in the accelerated carbonation chamber before starting the corrosion experiments. After carbonation, the corrosion specimens were removed from the chamber and then exposed to alternate wetting/drying cycles which were similar to chloride-induced corrosion but using tap water instead of sodium chloride solution. In addition, the passive condition was evaluated by monitoring specimens immersed in tap water for 6 weeks without any aggressive ions contamination (CO_2 and Cl^-) and then subjected to similar wetting/drying cycles with tap water.

2.3. Mechanical, physical and durability properties, pH and pore solution composition

Mechanical properties including compressive strength, indirect tensile strength and modulus of elasticity were measured on standard cylinders following ASTM C39, C469 and C496 respectively [32–34]. Physical and durability properties including water absorption, ultrasonic pulse velocity (UPV), volume of permeable void (VPV), sorptivity, surface and bulk resistivity were determined in compliance with ASTM C597, ASTM C642, ASTM C1585 and AASHTO TP95 respectively [35–38]. The detailed testing protocols for above experiments were reported in previous works of the authors [24,39].

According to previous study conducted by the authors [24], pH and pore solution composition were measured by using paste. Paste specimens were cured in airtight containers to maintain saturated conditions over the first 7 days and then stored in controlled room at 23 ± 2 °C and 50 ± 3% RH until 28 days, aiming to prevent leaching [24]. Pore solution was obtained by following a pore solution extraction method [40]. Subsequently, the pH was measured using a calibrated pH probe and ions concentration in pore solutions was analysed by Inductively Coupled Plasma Optical Emission Spectroscopy (ICP-OES).

2.4. Chloride content and carbonation depth measurement

Concrete powder was collected utilizing a Germann Profile grinder for every 1 mm until the depth of concrete cover (15 mm). ASTM C1152 [41] standard was adopted to determine acid soluble chloride which represents the total amount of chloride in the system. According to previous study, an ultrasonic bath instead of magnetic hot plate was employed to boil the testing solution to make chloride ions reactive and dissolve into solution for titration process [42]. The total chloride content was presented as percentage of binder mass at the rebar-concrete interface (15 mm).

Carbonation front penetration was monitored using 50 mm height concrete discs cut from standard cylinders. The circumference disc area was covered by self-adhesive aluminium foil to assure the carbonation occurs only from the top and the bottom bases. The concrete discs were subjected to the same exposure conditions as that of corrosion samples. At several time intervals, at least two discs were taken out of the carbonation chamber, split and tested using 1% concentration phenolphthalein solution. In addition, carbonation depth was determined by the average value of different location measurements excluding zones within 10 mm from the foil edge due to possible leakage effect [19]. When carbonation depth was reached, corrosion specimens were removed from the carbonation chamber and electrochemical experiments were conducted. In the end of the testing period, corrosion specimens were also split and exposed to 1% phenolphthalein solution on the fractured surfaces to validate the carbonation front penetration assessment.

2.5. Electrochemical experiments

All electrochemical tests were conducted utilizing a VMP3 Multichannel potentiostat in a controlled room with fixed temperature of 23 ± 2 °C. Three electrode system including reinforcement as working electrode (WE), Saturated Calomel Electrode (SCE) as reference electrode (RE) and Titanium mesh as counter electrode (CE) was used to carry out all experiments. The current interruption (CI) technique was utilized to compensate the ohmic drop (IR) due to electrolyte resistance and 85% of measured IR value was compensated to prevent the

Table 3
Mechanical, physical and durability properties of LC3 concrete.

Properties at 28 days	LC3	GP cement [24]	GP cement [49]
Compressive strength (MPa)	49.33 ± 1.39	52.3 ± 1.11	52.9 ± 1.0
Slitting tensile strength (MPa)	4.39 ± 0.08	4.6 ± 0.1	–
Elastic modulus (GPa)	34.5 ± 0.6	31.1 ± 0.9	32.2
Water absorption (%)	6.86 ± 0.17	–	6.3
UPV (m/s)	4551.1 ± 27.0	4508	3910
VPV (%)	15.83 ± 0.46	–	14.9
Initial rate of sorptivity ($\times 10^{-3}$ mm/s$^{0.5}$)	2.53 ± 0.16	–	2.9
Secondary rate of sorptivity ($\times 10^{-3}$ mm/s$^{0.5}$)	0.98 ± 0.11	–	–
Surface resistivity (kΩ-cm)	23.32 ± 0.68	19.4	12.0
Bulk resistivity (kΩ-cm)	13.03 ± 0.32	–	4.96

instrument from oscillation. During all electrochemical experiments, the specimen was immersed partially in tap water to avoid the limited oxygen diffusion. In addition, RE and CE were also placed in water next to corrosion specimens.

The first electrochemical test was carried out to determine an appropriate sweep rate (SR) to attain a quasi-steady-state condition for potential/current interaction in corroding flash calcined clay limestone blended OPC-based system. The high sensitivity of electrochemical protocols was widely employed to measure significantly small corrosion rates, especially in passive stage of reinforcing rebars. However, fast or slow SR causes the underestimation or overestimation of polarization resistance (R_p), resulting in inaccurate corrosion rate calculation [43]. A potentiodynamic cycles known as cyclic voltammetry (CV) protocols in potentiostat was carried out to investigate the effect of SR on reinforcing bars in both passive and active corrosion condition. The magnitude of ± 10 mV around the corrosion potential of specimens ($\Delta E = \pm 10$ mV) was used as the beginning and end of cycles. A broad set of SR from 1 to 1000 mV/min (0.00017 to 0.01667 V/s) were applied. The potentiodynamic cycles provided a potential-current (E-I) diagram for each SR value. The apparent resistance $R_{app} = R_p + R_e$ with R_e representing the electrolyte resistance was determined by the slope at the beginning of potential excursion. Subsequently, in the R_{app} and SR diagram, an appropriate SR was selected when R_{app} value obtained a constant value.

After obtaining suitable SR, open circuit corrosion potential (E_{corr}) and polarization resistance (R_p) of reinforcing steel bars were measured by well-established methodology linear polarization resistance (LPR) [44]. E_{corr} identified as the potential differences between the reinforcement (WE) and RE when deviation during 1 min was lower than 1 mV to ensure the stability of potential. The R_p was calculated based on the linear slope in polarization curve very near E_{corr} [45]:

$$R_p = \left(\frac{\Delta E}{\Delta I}\right)_{\Delta E \to 0} \quad (1)$$

A potentiodynamic scanning from -20 mV to 20 mV around E_{corr} ($\Delta E = \pm 20$ mV) was applied to detect the response from corroding system (ΔI) for R_p calculation. For active specimens, E_{corr} and R_p were recorded every 3 weeks in the end of immersion duration in sodium chloride solution or tap water for chloride and carbonation-induced rebars corrosion respectively. Passive samples were first measured E_{corr} and R_p at 42 days in tap water and several times at the end of wetting cycles. The testing duration was about 500 days for both active and passive samples.

Tafel plot known as the intersection method from the extrapolation of the anodic and cathodic linearity was employed to simultaneously determine corrosion current (I_{corr}) and Tafel constant via Stern-Geary equation [44]:

$$B = \frac{\beta_a \beta_c}{2.3 \times (\beta_a + \beta_c)} \quad (2)$$

where β_a and β_c are the anodic and cathodic Tafel constants calculated as slopes of anodic and cathodic linear sections from the Tafel plot of I_{corr} logarithm and overpotential. In this study, the large overpotential from -250 mV to 250 mV ($\Delta E = \pm 250$ mV) was utilized to obtain Tafel plots. However, due to limitation of Tafel test being a destructive test causing permanent alteration for equilibrium condition of corroding system, it was performed only at specific times throughout the entire experiment duration.

After conducting Tafel tests on specific specimens, gravimetric mass loss quantifications following ASTM G1 were carried out to validate the electrochemical parameters previously selected. Reinforcing bars were removed by splitting corrosion specimens and slightly cleaned from remaining concrete residue on the steel surface. A reagent grade chemical composition of 1000 ml hydrochloric acid (HCl with specific gravitiy of 1.19), 20 g antimony trioxide (Sb_2O_3) and 50 g stannous chloride ($SnCl_2$) was selected as chemical procedures under testing temperature of 23 ± 2 °C. The experimental solution was vigorously stirred by magnetic stirrer during the immersion of reinforcements for 20 to 25 min. Subsequently, the rebars were removed from the cleaning solution, gently brushed to eliminate corrosion products and weighed to record the mass losses. This procedure was repeated at several times on specimen to form a plot of mass loss vs. the number of cleaning cycles for each reinforcing bar. The mass loss induced by corrosion process was determined at the point that the graph begins plateau [30]. After this point, mass losses are considered as the removal of base metal in steel bar after corrosion products being completely removed.

3. Results and discussion

3.1. Mechanical, physical and durability properties

Table 3 presents the characteristics of the LC3 concrete including mechanical, physical and durability properties. The compressive strength of the LC3 concrete with 20 wt% GP cement replacement (28 wt% OPC replacement) complies with Australian Standard (AS 3600 [46]), American Concrete Institute (ACI 318 [47]) and European Standard (EN 206 [48]) specification in chloride environments. LC3 concrete performs similarly to conventional OPC concrete in terms of water absorption, UPV, VPV and sorptivity properties. Noticeably, LC3 concrete resistivity including both surface resistivity and bulk resistivity is significantly higher than that of GP cement concrete with similar compressive strength [24,49].

3.2. Steel bars depassivation

After oven-drying the specimens and 7 days in sodium chloride solution, the total chloride content at the depth of reinforcing bars (15 mm) was measured reaching 0.2% by mass of binder (Fig. 2). At the same time, the average corrosion potential was in the range of uncertain corrosion activity (Fig. 2), which indicates that the steel bars might not be depassivated. As a result, the oven-drying and chloride solution immersion cycles were repeated several times and corrosion

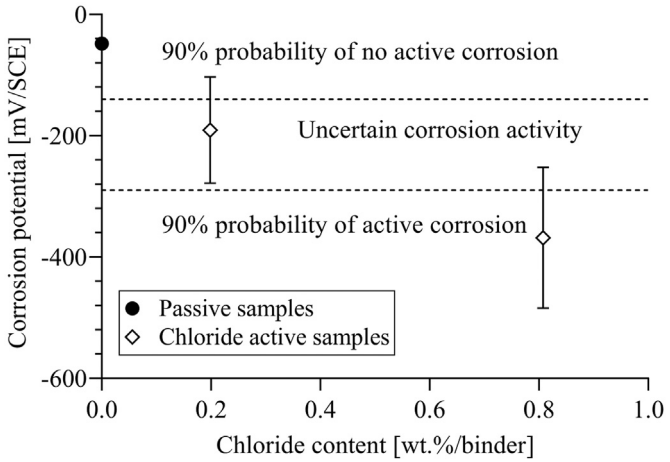

Fig. 2. Variation of corrosion potential versus total chloride content at steel-concrete interface.

potential was monitored until depassivation of steel. After 4 cycles, the average corrosion potential entered in the 90% probability of corrosion activity zone with the chloride content of 0.8 wt% of binder (Fig. 2).

The carbonation depth of samples from 1st and 2nd set exposed to 1% CO_2 and 55% RH are presents in Fig. 3 together with photos of phenolphthalein indicator test results. After 238 days, the carbonation front reached at the interface between steel and concrete, leading to the depassivation of the steel bar (Fig. 3a). This 1st set of carbonation corrosion specimens was removed from carbonation chamber and subjected to alternate wetting/drying cycles in tap water for electrochemical experiments. The 2nd set of specimens was exposed to carbonation up to 284 days to achieve carbonation depth leading to the depassivation of the whole steel bar (around 16.21 ± 0.21 mm) for the investigation of long-term corrosion process (Fig. 3b). After conducting the phenolphthalein indicator test, the 2nd set of specimens was also exposed to similar wetting/drying cycles.

3.3. Sweep rate from potentiodynamic cycles

Fig. 4 summarizes the effect of different SR on apparent polarization resistance (R_{app}) of corrosion samples containing flash calcined clay and limestone. The R_{app} values of passive, chloride and carbonation-induced active samples were deduced from the potentiodynamic cycles obtained using different SR. Fig. 4(a) presents an example of response to triangular wave of potential in passive samples in the form of potential-current (E-I) diagram. In the E-I diagram, $1/(R_e + R_p)$ was calculated as the slope at the beginning of potential excursion. Hence, different SR received different responses from the corroding system, resulting in the variation of R_{app} from R_e to $R_e + R_p$. To eliminate the inaccuracy in calculation of corrosion rate (relating to I_{corr}), an appropriate SR must be selected to obtain the constant R_{app} value [43,50].

Fig. 4(b) illustrates the alteration of R_{app} in term of sweep rate from 0.5 mV/min to 1000 mV/min. The CV test was conducted after 250 days in passive condition on reference passive specimens (not exposed to chloride and carbonation). Active corrosion specimens (both chloride- and carbonation-induced) were tested after 250 days of wetting/drying cycles. A plateau was noticed in the SR between 5 mV/min to 10 mV/min for passive samples and another insignificant variation of SR was observed at very high SR larger than 500 mV/min corresponding to the value of R_e. The constant R_{app} magnitude at SR from 5 mV/min to 10 mV/min was also detected on active samples but the decreasing rate of R_{app} from the beginning to the end of the SR spectrum was very low compared to passive samples, particularly for chloride-contaminated corrosion. In addition, the lowest R_{app} amplitude of chloride active samples can be attributed to the immersion of these samples into simulated salt water (35 g/l sodium chloride solution) which is very conductive. Considering all these SR evaluations, 10 mV/min SR was selected to perform all electrochemical experiments

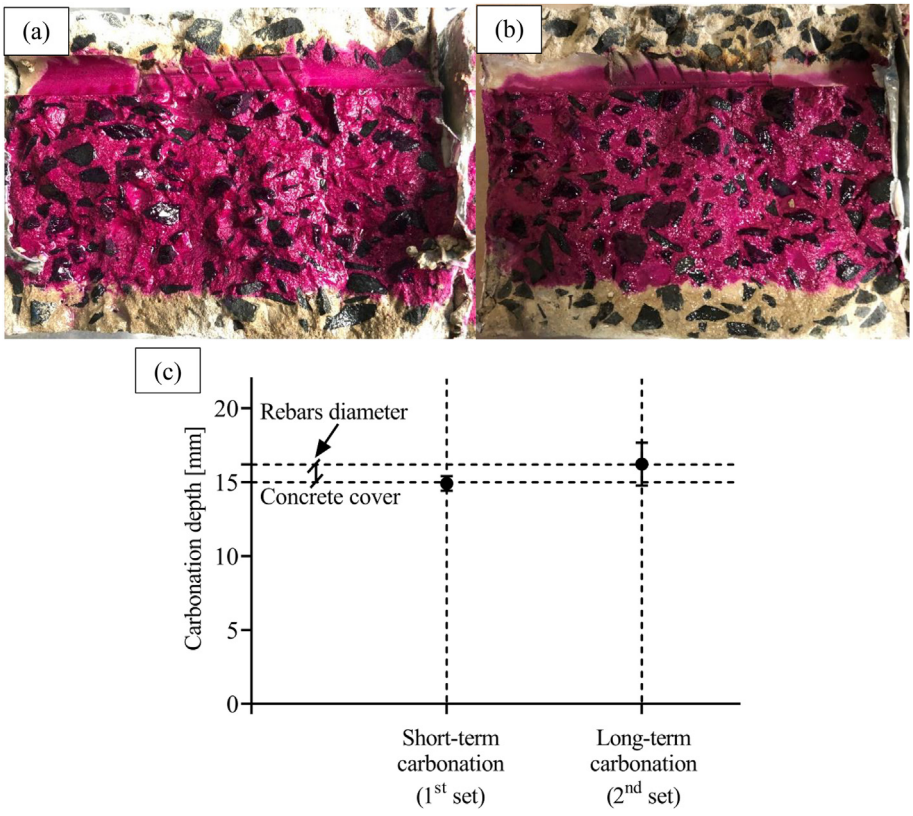

Fig. 3. (a) Photo of 1st set of active sample. (b) Photo of 2nd set of active sample. (c) Average carbonation depth of carbonation-induced corrosion samples.

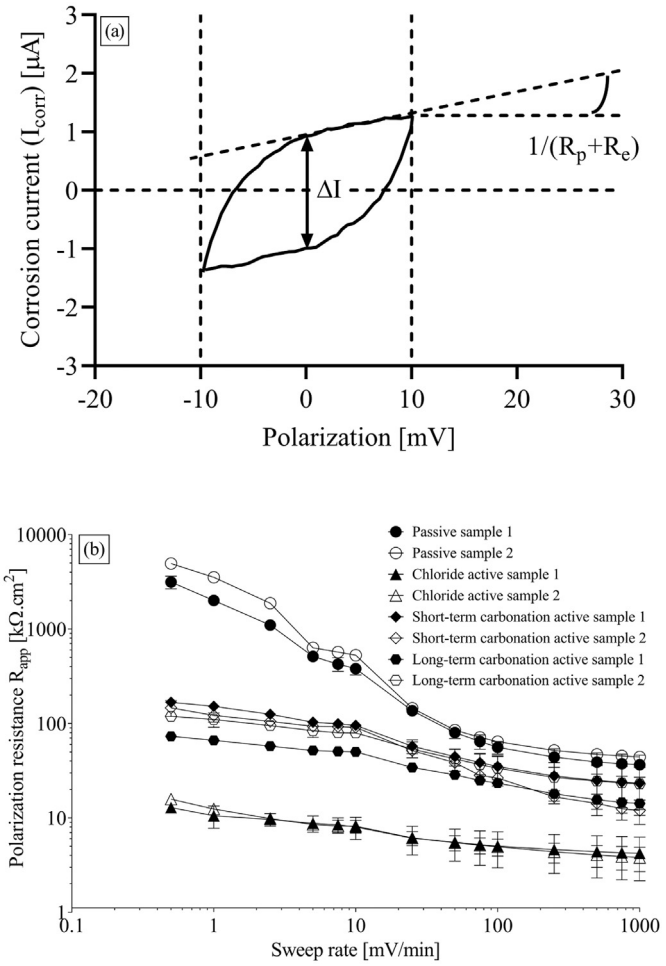

Fig. 4. (a) An example of current response to triangular wave of potential in passive samples. (b) Relationship between sweep rate and apparent polarization resistance.

for both passive and active samples in this study. The 10 mV/min SR also satisfies the recommendable maximum SR for steel corrosion in concrete [43].

3.4. Corrosion potential and polarization resistance

E_{corr} measured via open circuit potential are presented in the Fig. 5 for both passive and active corrosion samples up to 500 days. E_{corr} measurement is one of the most common protocols to monitor corrosion either in the laboratory or real reinforced concrete structures. It is also a well-developed technique over 40 years, standardized as ASTM C876 [51]. However, the drawback of E_{corr} is to provide only a qualitative assessment, which does not allow deducing the corrosion rate of reinforcement. The time-dependent evolution of E_{corr} was monitored on all specimens but only the average values of E_{corr} are represented calculated from either two or three acquired points due to the destructive Tafel test conducted throughout the exposure duration on both passive and active specimens. E_{corr} values from reference plain OPC specimens are also reported in Fig. 5 from previous study [52]. Despite the slightly different exposure condition compared to this study, the values for E_{corr} from Aguirre-Guerrero et al. [52] were considered for comparison purpose together with the classification from ASTM C876 based on value versus copper-copper sulfate reference electrode (CSE). The corrosion potential measurements in this study and in previous study [52] were carried out using the saturated standard calomel electrode (SCE) and Ag/AgCl/sat KCl reference electrode respectively. Thus, for comparison purpose, 60 mV were added to classification from ASTM C876 whilst measured values on plain OPC concrete [52] were reduced by 45 mV to be integrated into Fig. 5.

Regarding passive samples, E_{corr} value for the first and second measurement was around -75 mV after 42 days immersion in tap water. Then, E_{corr} of passive specimens increased and slightly fluctuated between -40 mV to -30 mV until 500 days, which indicates that E_{corr} magnitude of samples containing flash calcined clay and limestone remained in the range of over 90% probability of having no corrosion. Overall, the ASTM C876 classification in passive state for conventional OPC concrete can be also utilized to identify passive state of LC3 concrete.

For chloride contaminated active samples, as shown in Fig. 5, corrosion potential of LC3 concrete from initial -368 mV reduced to -454 mV and -504 mV after the second and third cycles in sodium chloride solution respectively. Eventually, E_{corr} only marginally decreased fluctuating insignificantly between -570 mV to -610 mV after 239 days to 500 days. OPC concrete with relatively similar exposure procedure (15 days of immersion in 3.5% NaCl solution and 15 day of drying after accelerated initiation phase [52]) exhibited a lower E_{corr} at the start of the testing period but the reduction rate was superior to that of LC3 concrete. Hence, E_{corr} values were comparable after about 270 days in propagation phase for OPC and LC3 concrete.

E_{corr} evolution of the two carbonated corrosion sample sets is also shown in Fig. 5. The two sets of carbonated specimens presented a similar trend in corrosion potential from 7 days to 500 days of exposure with values rising from -461 mV and -504 mV to about -249 mV and -292 mV for the 1st and 2nd set of samples respectively. The E_{corr} increased during the testing period could be explained by the availability of CO_2 at the steel-concrete interface. The presence of carbon dioxide mediates in pH reduction of the interfacial zones accelerating not only the acidification in anodic reaction but also the reaction rate in cathodic areas [8]. In the beginning, large quantity of CO_2 was available leading to high absolute values of corrosion potential. Then, during the wetting/drying cycles, CO_2 diffused from the inner part of specimens with high CO_2 concentration to ambient environment with low CO_2 concentration, leading to a reduction in CO_2 inside the specimens resulting in higher values of corrosion potential. Nevertheless, the differences between E_{corr} value of passive samples and CO_2-active samples were higher than 150 mV allowing to distinguish passive and active corrosion sample as the recommendation from RILEM technical committee (TC) 235-CTC [53]. A comparison with values obtained on plain OPC concrete is also presented in Fig. 5 although OPC samples were continuously placed in an environmental chamber at 1% CO_2 concentration [52]. At the beginning of the depassivation period of reinforcing bars, OPC concrete specimens produced higher E_{corr} values compared to LC3 concrete and fluctuated in the uncertain corrosion activity zone until 240 days. E_{corr} was almost constant OPC concrete specimens due to continuous availability of CO_2 in the chamber. Interestingly, throughout the exposure duration, the significant differences in E_{corr} between the 1st set and 2nd set of specimens were observed. The 2nd set presented a lower corrosion potential than that of the 1st set since the 2nd set specimens experienced longer CO_2 exposure duration leading to deeper carbonation front penetration and lower pH environment around steel-concrete interface as reported in previous study [54]. Overall, corrosion potential classification from ASTM C876 can be used in concrete containing flash calcined clay and limestone.

Fig. 6 shows the evolution of the polarization resistance up to 500 days at both passive and active specimens. The counterpart values of OPC concrete from previous studies were also presented for comparison purpose [29,52]. Linear polarization resistance (R_p) is widely considered as convenient and reliable technique which allows to routinely measure corrosion in reinforced concrete structure. It is also the most preferable protocol to quantify metal loss in corrosive reinforcement or any metal/electrolyte systems. In R_p measurement, consistent polarization potential (ΔE) around 20-30 mV (20 mV in this study) is

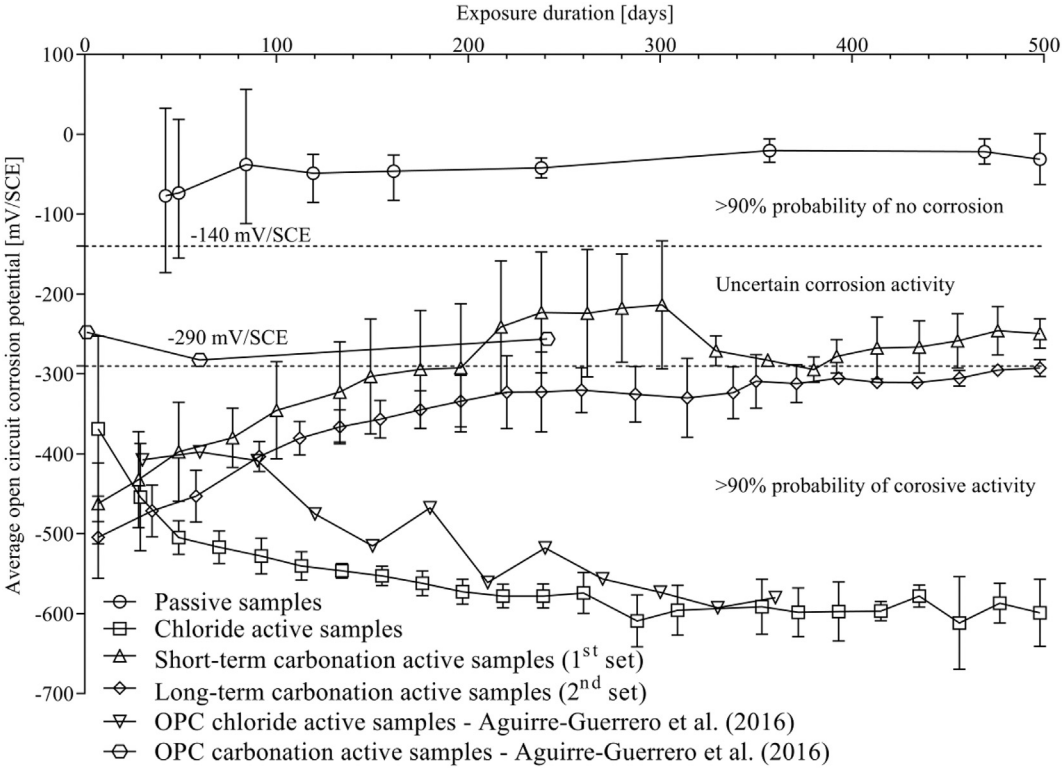

Fig. 5. Variation of open circuit corrosion potential of LC3 and reference benchmark of OPC.

applied to obtain the polarization current (ΔI) from polarization curve. Insignificant overpotential together with relatively shorting measuring time does not generate irreversible change in the corroding system until next measurement, for instance three weeks in this study. Thus, polarization resistance measurements can be repeated throughout the entire exposure period. The corrosion rate classification based on R_p values of plain OPC concrete from polarization curve [55,56] is also integrated in Fig. 6. The polarization resistance for OPC concrete active

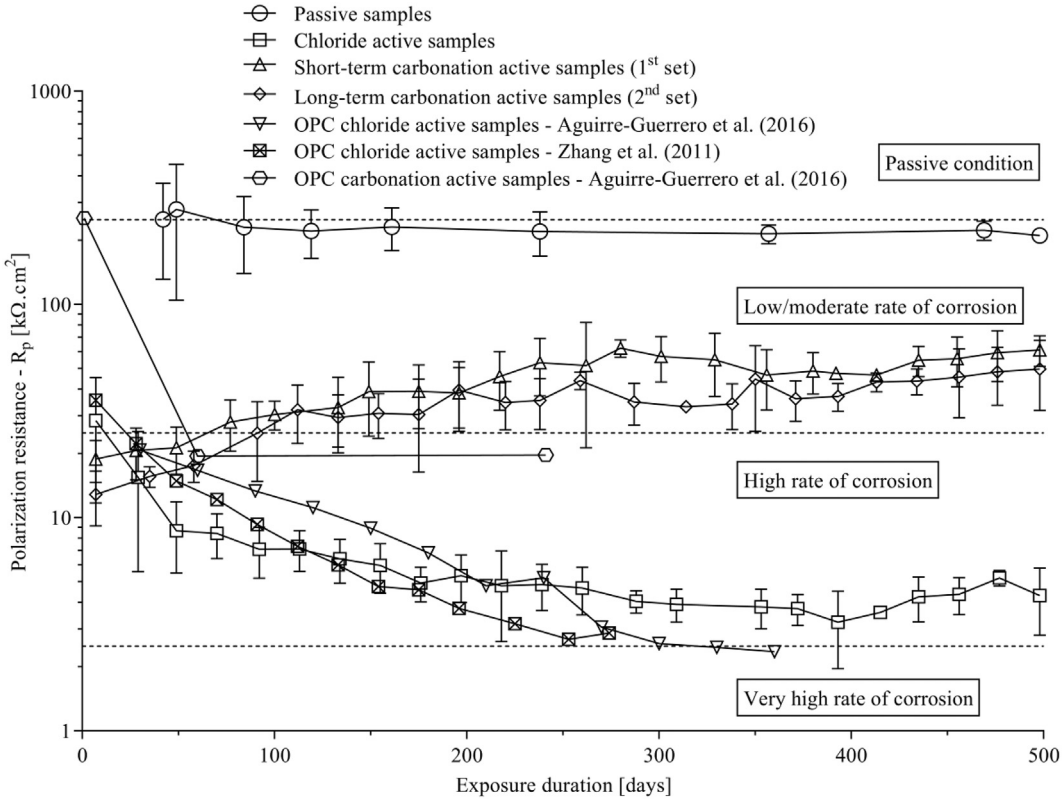

Fig. 6. Evolution of polarization resistance of LC3 concrete and reference benchmark of OPC.

corrosion specimens from Aguirre-Guerrero et al. [52] was derived from "B" coefficient of 26 mV dividing by corrosion rate (i_{corr}). Another study from Zhang et al. [29] with similar alternating wetting/drying cycles for chloride-induced specimens was also considered to compare with this study. Although Zhang et al. [29] investigated the influence of the top-bar effect, only the average R_p value of five reinforcing bars located at the bottom of the concrete walls with no interface defects was considered.

The polarization resistance measured in LC3 concrete passive specimens was overall slightly lower than that of passive condition classification for OPC concrete (Rp ~250 kΩ.cm^2). The fluctuation was insignificant in comparison with corrosion potential values with an average amplitude being around 220–230 kΩ.cm^2. Consequently, a recalibration of R_p classification in passive condition might be required for LC3 concrete.

In chloride-induced reinforcement corrosion, the average R_p amplitude from both OPC and LC3 concrete exhibited similar decreasing trend over the entire testing period. The value of polarization resistance of LC3 concrete was remarkably reduced from 35.5 kΩ.cm^2 to 8.7 kΩ.cm^2 in the first to third cycles in exposure to NaCl 35 g/l and then decreased moderately until 218 days. After that, the R_p remained fairly stable around 4.5 kΩ.cm^2. It is worth to mention that plain OPC concrete specimens adapted from previous studies [29,52] showed very high corrosion rates with R_p values < 2.5 kΩ.cm^2 whilst LC3 concrete specimens remained in the zone of high corrosion rate (2.5 kΩ.cm^2 < R_p < 25 kΩ.cm^2). Consequently, during the propagation phase of chloride-induced reinforcement corrosion, combination of flash calcined clay and limestone performed similarly or better than conventional OPC concrete.

The polarization resistance of carbonated specimens displayed an increasing trend versus time with R_p values rising from high rate of corrosion to low-moderate corrosion rate (Fig. 6). The R_p value from the 1st and 2nd set of carbonation active sample marginally stabilized after 240 days of exposure time. As mentioned for corrosion potential values, the increasing trend in average R_p values can be attributed to the gradually CO_2 disappearance within the interfacial reinforcement-concrete area [57]. Plain OPC concrete [52] showed a lower polarization resistance of 19.7 kΩ.cm^2 up to 240 days. The gap in terms of the polarization resistance of 1st set and 2nd set was also noticed but the difference was not obvious as corrosion potential.

The relationship between corrosion potential and polarization resistance is reported in Fig. 7 with 339 independent data points measured by LRP technique in both passive and active samples during the entire testing period. A decreasing trend of R_p value with the decrease in corrosion potential was undoubtedly observed. Moreover, an exponential equation could be established correlating R_p and E_{corr} with a good correlation coefficient (R^2 = 0.9) as follows:

$$R_p = 293.4e^{0.006653 \times E_{corr}} \quad (3)$$

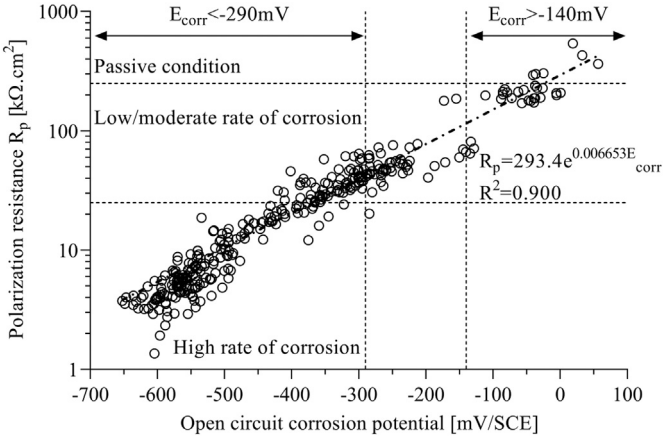

Fig. 7. Exponential correlation between corrosion potential and polarization resistance.

Exponential-like tendency in the evolution of polarization resistance depending on corrosion potential was reported in previous studies for either plain OPC concrete or concrete containing binder replacement including silica fume, fly ash and ground granulated blast furnace slag by means of corrosion current density and corrosion potential correlation [58–60].

The corrosion potential and polarization resistance classifications are also displayed in Fig. 7. There was no "false positive" data point (E_{corr} < -140 mV but R_p > 250 kΩ.cm^2) observed in > 90% probability of no corrosion and uncertain corrosion activity zones. In addition, 260 out of 308 data points located in "absolute negative" zone (E_{corr} < -290 mV and R_p < 250 kΩ.cm^2) included about 84.4% of active corrosion measurement, which indicates the reasonable reliability of corrosion assessment for corrosion potentials less than -140 mV. On the other hand, within 31 data points counted in passive condition zone (E_{corr} > -140 mV), no "false negative" values (E_{corr} > -140 mV but R_p < 25 kΩ.cm^2) was recorded. However, only 6 measurements created "absolute positive" data point (E_{corr} > -140 mV and R_p > 250 kΩ.cm^2), representing only 19.4% of the counts in passive classification. Hence, this phenomenon confirmed that, for re-calibration in passive condition, further studies regarding electrochemical behaviours in passive state of concrete containing flash calcined clay and limestone is recommended.

To provide more insightful evaluation on the relationship between corrosion potential and polarization resistance, single-factor analysis of variance (ANOVA) was performed including data points. The outcomes of ANOVA are summarized in Table 4 with 95% confidence interval for R_p average. The polarization resistance measurements were divided into 13 classes with 50 mV of corrosion potential range from -600 mV to -50 mV. Only 2 clusters from -200 mV to -100 mV produced significant differences in standard deviation due to the small number of samples (only 6 measurements in each potential section). Considering polarization resistance values in 95% confidence intervals in other potential classes together with F-statistic parameters at 161.2 (remarkably higher than 1) indicating independent R_p value in each potential group, it can be concluded that the polarization resistance alteration is statistically related to the evolution of corrosion potential. Overall, a correlation between polarization resistance and corrosion potential in LC3 concrete can be rationally established, providing the possibility to employ corrosion potential monitoring as a semi-quantitative and efficient assessment of steel depassivation.

Table 4
ANOVA analysis summary with 95% confidence interval for R_p average.

	F-statistic	*p*-Value	R^2
ANOVA summary	161.24	< 0.0001	0.8558
E_{corr} range (mV/SCE)	Data points (count)	Average R_p (kΩ.cm^2)	R_p range with 95% confidence interval (kΩ.cm^2)
< −600	21	3.71	3.35 to 4.07
−600 to −550	62	5.13	4.77 to 5.49
−550 to −500	51	7.62	6.72 to 8.51
−500 to −450	25	11.99	10.56 to 13.42
−450 to −400	21	21.44	18.12 to 24.75
−400 to −350	33	28.28	25.40 to 31.16
−350 to −300	35	37.82	34.78 to 40.86
−300 to −250	40	46.79	43.50 to 50.08
−250 to −200	12	57.90	50.73 to 65.07
−200 to −150	6	95.11	23.76 to 166.5
−150 to −100	6	91.93	36.94 to 146.9
−100 to −50	9	203.00	189.2 to 216.8
> −50	18	257.86	208.0 to 307.7

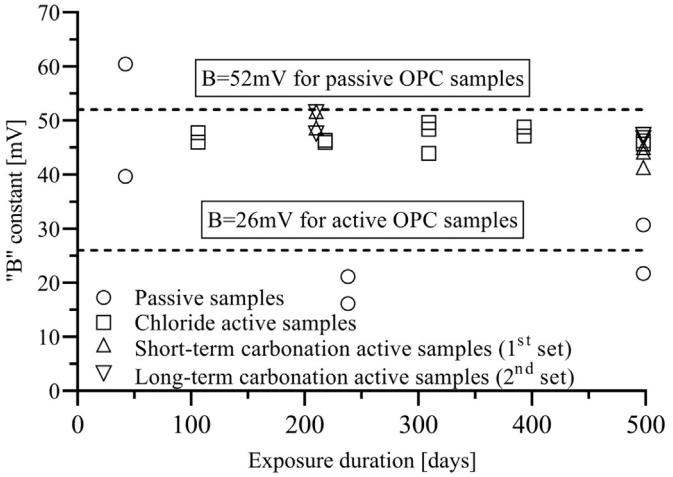

Fig. 8. Evolution of Tafel B constant and suggested value of OPC from Ref. [62].

3.5. Tafel "B" constant and corrosion current density

In terms of corrosion rate determined by linear polarization resistance technique, as shown in Stern-Geary equation (Eq. (2)), the "B" constant is governed by two parameters: anodic and cathodic Tafel constants. It is also necessary to evaluate the Tafel constant for corroding system combining flash calcined clay and limestone in binder composition. These constants were obtained from the extrapolation of the anodic and cathodic branches of the polarization curves applying a large over-potentials above corrosion-free potential ($\Delta E = \pm 250$ mV). However, due to the destructive nature of "Tafel extrapolation" approach, this technique was conducted only two to five times for passive, chloride and carbonated samples over the entire exposure duration. All results from Tafel plots are reported in Fig. 8 and Table 5 as anodic, cathodic and B Tafel constants.

β_a, β_c and B coefficients were systematically evaluated via theoretical analysis in a previous study for OPC concrete. Song [61] reported four different types of polarization condition occurring in reinforced concretes due to different anodic and cathodic reaction rates. In case of LC3 concrete in this study, active and passive state without oxygen diffusion rate-determining factor (transport of oxygen not controlling the reaction rate in reinforcements due to alternating wetting/drying cycles) are considered as the two types of possible electrochemical behaviours. In the former state, the corrosion process of rebars can consider as oxidation of steel at the anode and oxygen reduction at the cathode: redox reaction within "corrosion cell" [8]. The anodic Tafel slopes can be estimated approximately at 30-39 mV due to the Tafel slope of iron in NaOH solution with pH value higher than 13 at 20 °C. On the other hand, the cathodic Tafel slope is dominantly subjected to cathodic processes consisting of oxygen reduction and hydrogen evolution. To be more specific, the β_c value range for oxygen reduction depending on the pH value of the electrolyte and the hydrogen evolution in sodium hydroxide is 48-120 mV and 120-150 mV respectively. In general, with the estimation of 30 mV $\leq \beta_a \leq$ 39 mV and 48 mV $\leq \beta_c \leq$ 150 mV, Tafel B constant fluctuates from 8 to 13.5 mV (8 mV $\leq$ B $\leq$ 13.5 mV). Regarding passive state, with sufficient oxygen at reinforcement-concrete interfacial zone, anodic Tafel constant is estimated to be infinity whilst cathode is predominantly governed by oxygen reduction process with the cathodic β_c constant as mentioned above in the range of 48-120 mV. Consequently, B constant in this case is approximately equivalent to $\beta_c/2.3$ (21 mV $\leq$ B $\leq$ 52 mV).

All data points presented in Fig. 8 are reported in Table 5 which also includes anodic and cathodic Tafel coefficients to provide more insightful understanding of corrosion kinetics of LC3 concrete. The curve-fitting analysis using the least Chi-squared (χ^2) method was performed to calculate β_a and β_c based on the slopes in anodic and cathodic linear sections of fitted curve. Subsequently, the "B" Tafel values were determined following Eq. (2). The variation of B coefficient over the testing period is illustrated in Fig. 8. For passive samples, B constant showed higher amplitude after 42 days of continuous immersion in tap water (39.7 mV and 60.5 mV) than that obtained for longer exposure duration (ranging from 16.1 mV to 30.7 mV). As a result, Tafel values for passive specimens seem to be dependent on the environmental storage condition of the specimens which is constant with Song's recommendation [61] as 4 out of 6 passive Tafel plot measurements positioned within the theoretical B coefficient range proposed by Song [61]. By contrast, both chloride and carbonation-induced active samples reported insignificant fluctuation during the whole testing period. The average B value together with the standard deviation and the coefficient of variation are 47 mV, 2.48 and 0.05 respectively for the entire active samples data group, which indicates a stabilization of anodic and cathodic reactions during corrosion process from the beginning of the exposure period up to 500 days.

Table 5
Anodic, cathodic and "B" Tafel constants for both passive and active specimens.

Duration (day)	Anodic constant β_a (mV)	Cathodic constant β_c (mV)	B constant (mV)
Passive samples			
42	∞	91.2	39.7
42	∞	139.1	60.5
238	∞	37.1	16.1
238	∞	48.6	21.1
500	∞	70.6	30.7
500	∞	50.0	21.7
Chloride active samples			
106	274.9	182.9	47.75
106	271.8	173.0	45.96
218	277.1	170.7	45.93
218	298.5	165.6	46.31
309	267.3	162.4	43.92
309	287.9	189.1	49.62
309	302.9	175.9	48.38
393	273.0	179.8	47.13
393	282.3	186.3	48.80
500	299.5	161.7	45.66
500	267.8	176.3	46.22
Short-term carbonation active samples (1st set)			
210	280.6	185.8	48.60
210	275.3	209	51.65
500	344.0	144.0	44.13
500	386.5	141.2	44.96
500	303.7	138.4	41.34
Long-term carbonation active samples (2nd set)			
210	277.5	206.9	51.53
210	287.1	176.7	47.56
500	276.4	179.5	47.32
500	306.4	165.6	46.74

Previous study conducted substantial experimental works on different types of cement including OPC, slag cement and pozzolanic cement with or without depassivating and inhibitor additives [62]. B = 26 mV in active state and B = 52 mV in passive state for bare steel were suggested via various comparison between gravimetric and electrochemical mass loss calculated from LRP method as well as exposure conditions, which also integrates into Fig. 8. These B coefficient values were then widely accepted to quantify the corrosion rate in both laboratory studies and existing reinforced structures. Andrade and Gonzalez [62] also explained the dissimilarities between the gravimetric mass loss and electrochemical counterpart values due to uncompensated IR-drop but now this difficulty can be efficiently solved by automated IR-drop compensation in current potentiostat. However, a wide range of β_a, β_c and B parameters were reported in current literature. Locke and Siman [63] revealed that the variation in anodic and cathodic Tafel constants can range from 320 mV to 1570 mV and

380 mV to 1080 mV respectively resulting in parameter B varying within 76 mV to 278 mV. Garces et al. [64] reported a fluctuation of the B coefficient from 21 mV to 37 mV in different pH solutions (acid and neutral solution) with or without chloride ions simulating the concrete pore solutions. Chang et al. [65] investigated the polarization behaviours of reinforcement in fly ash and slag cement concretes showing that the β_a, β_c and B coefficients could vary in the range of 230 mV to 800 mV, 192 mV to 263 mV and 52 mV to 86 mV respectively, which is much higher than the estimated B amplitude of 26 mV for active specimen proposed by Andrade and Gonzalez [62]. A comparison between experimental data and numerical model by Michel et al. [66] also indicated significant variations in terms of anodic β_a and cathodic β_c Tafel constants in the amplitude of 10 mV to 369 mV and 10 mV to 233 mV respectively to provide the best fit for experimental corrosion current density.

In this study, the values of B did not agreed with the suggested values (B = 52 mV and B = 26 mV for passive and active samples respectively). For LC3 concrete passive samples, only one measurement presented relatively agreeing value (60.5 mV versus 52 mV) whilst other passive data provided lower B coefficient than 52 mV. In Table 5, all anodic Tafel constant of passive samples approached infinite value, indicating that parameter B was determined solely from cathodic Tafel constant β_c. More work is certainly required to re-calibrate the "B" coefficient in LC3 concrete passive stage. By contrast, carbonated and chloride active specimens displayed higher value than expected (47 mV compared to 26 mV). Andrade & Gonzalez [62] suggested the both β_a and β_c to be equal to 120 mV to generate a B coefficient of 26. The anodic and cathodic Tafel slopes of LC3 specimens were higher than 120 mV. Indeed, as shown in Fig. 9, electrochemical mechanism of reinforcement corrosion is principally governed by the current transport between reinforcing bars and concrete [67]. Specifically, anodic and cathodic processes are controlled by the current transport within concrete porosity and rebars. For cathodic regions, the flow of ions governs the transportation of current within concrete. Therefore, the ability of concrete to resist ions movement, known as electrical resistivity, appears to be controlling the cathodic process in active stage of reinforcement corrosion [8,67]. The electrical resistivity whereby surface and bulk resistivity of LC3 were noticeably higher than traditional OPC concrete [24] as also reported elsewhere [22]. The higher electrical resistivity induces lower charges transfer leading to higher cathodic Tafel slope as higher potential step perturbation is necessary to obtain a similar electrochemical behaviour. Regarding the transport of current within reinforcing bars, corrosion products located on the surface of reinforcement can work as a barrier for redox reaction. The iron oxide layers accumulating during corrosion process lead to conductivity loss in presence of water in rust [68], which reduces the transfer rate of electronic current. As a result, similarly to cathodic process, anodic Tafel slope can be higher than the suggested value of 26 mV in active phase.

One of the widely accepted indexes used to assess corrosion in reinforced concrete structures is the corrosion current density also known as corrosion rate ($\mu A/cm^2$). From corrosion rate, reinforcing bars cross-section loss and corrosion penetration can be calculated to predict the service-life of concrete member. To provide more insightful understanding of the corrosion of rebars, the evolution of the corrosion rate (corrosion current density) up to 500 days were deduced using two methods based on the linear polarization technique (LRP method from Section 3.4) by using either the conventional parameter B = 26 mV or the Tafel intersection technique (Section 3.5). The results are presented in Fig. 10. Corrosion rates from Tafel extrapolation method were simultaneously calculated using anodic and cathodic Tafel slopes (β_a and β_c) obtained by least Chi-squared curve-fitting analysis. For chloride-induced reinforcement corrosion, corrosion rate increased steadily from the beginning of the exposure period and plateaued after 218 days, remaining in the high corrosion rate zone up to 500 days. By contrast, for carbonated active specimens, the corrosion rate started at high rate of corrosion and then declined toward low or moderate corrosion rate category. The decreasing trend in corrosion rate is consistent with the increasing trend of open circuit corrosion potential and polarization resistance results. Explanation for this observed trend is detailed in Section 3.4. Overall, using the suggested B value of 26 mV for active specimens or "B" value deduced from Tafel intersection method led to comparable values of corrosion current densities. The only dissimilarities observed between the two methods were for chloride active corrosion samples at 106 days and 1st set of carbonated active specimens particularly at the end of testing period. The first explanation for these dissimilarities was the limited data obtained from the Tafel extrapolation plot. Indeed, only two or three Tafel measurements were conducted to acquire the corrosion rate (Table 5). Therefore, the Tafel intersection method cannot represent electrochemical behaviours of the entire sample set. Secondly, inaccurate estimation of the corroding area of the rebars can lead to corrosion rate miscalculation. Indeed, pitting corrosion in chloride active corrosion sample or reinforcement corrosion in 1st sample set involved only a limited corroding area of the steel bar surface. As a result, considering the whole area of rebars in the calculation of corrosion current density underestimated the corrosion rate [45,69]. The relationship between corrosion rate and polarization resistance can be expressed as follow [44,45]:

$$i_{corr} = \frac{B}{R_p} \quad (4)$$

The increase of B coefficient in Eq. (4) generates higher corrosion rates. Therefore, utilizing the measure B = 47 mV from Tafel intersection method instead of the proposed value of B = 26 mV from Gonzalez and Andrade [62] resulted in a larger corrosion rate leading to a more conservative evaluation of reinforcement corrosion. More research involving Tafel curve based assessment of B coefficient of concrete containing flash calcined clay and limestone as well as other SCMs should be carried out in order to provide more accurate structure durability design and assessment.

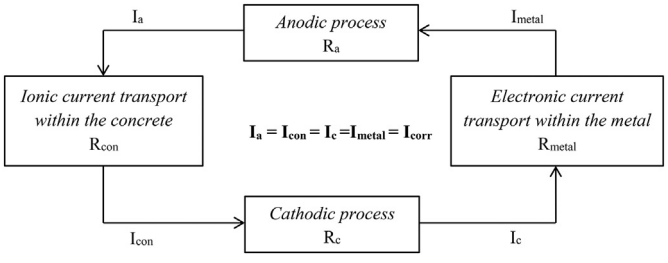

Fig. 9. Electrochemical mechanism of corrosion of reinforcements in concrete. (Adapted from [67,74]).

3.6. Gravimetric mass loss and corrosion pattern

Gravimetric mass loss measurements compared to electrochemical mass losses in Fig. 11. Gravimetric mass losses were determined on the specimens used for Tafel coefficients measurement. Steel bars were chemically cleaned using the ASTM G1 procedure. To obtain only the mass loss from corrosion process, six uncorroded steel bars extracted from passive specimens were subjected to same cleaning methodology to assess the mass of pre-existing oxides, which was then deducted from the total mass loss of corroded bars for both chloride or carbonated specimens. An average mass loss of 0.307 g with a standard deviation of 0.016 g was measured for passive samples.

Electrochemical mass loss was calculated by employing Faraday's law at various exposure periods as following:

$$m_{electrochemical} = \frac{A \times I_{corr} \times t}{n \times F} \quad (5)$$

where A is the atomic mass of metal (55.85 g/mol for iron), I_{corr} is the

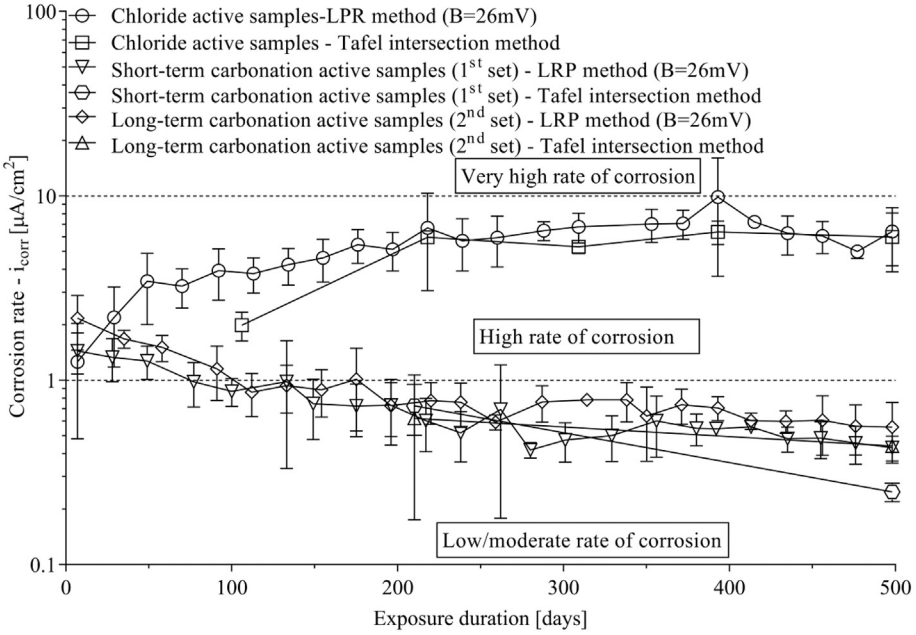

Fig. 10. Evolution of corrosion rate using two different calculation methods: Tafel intersection and LRP method with B = 26 mV.

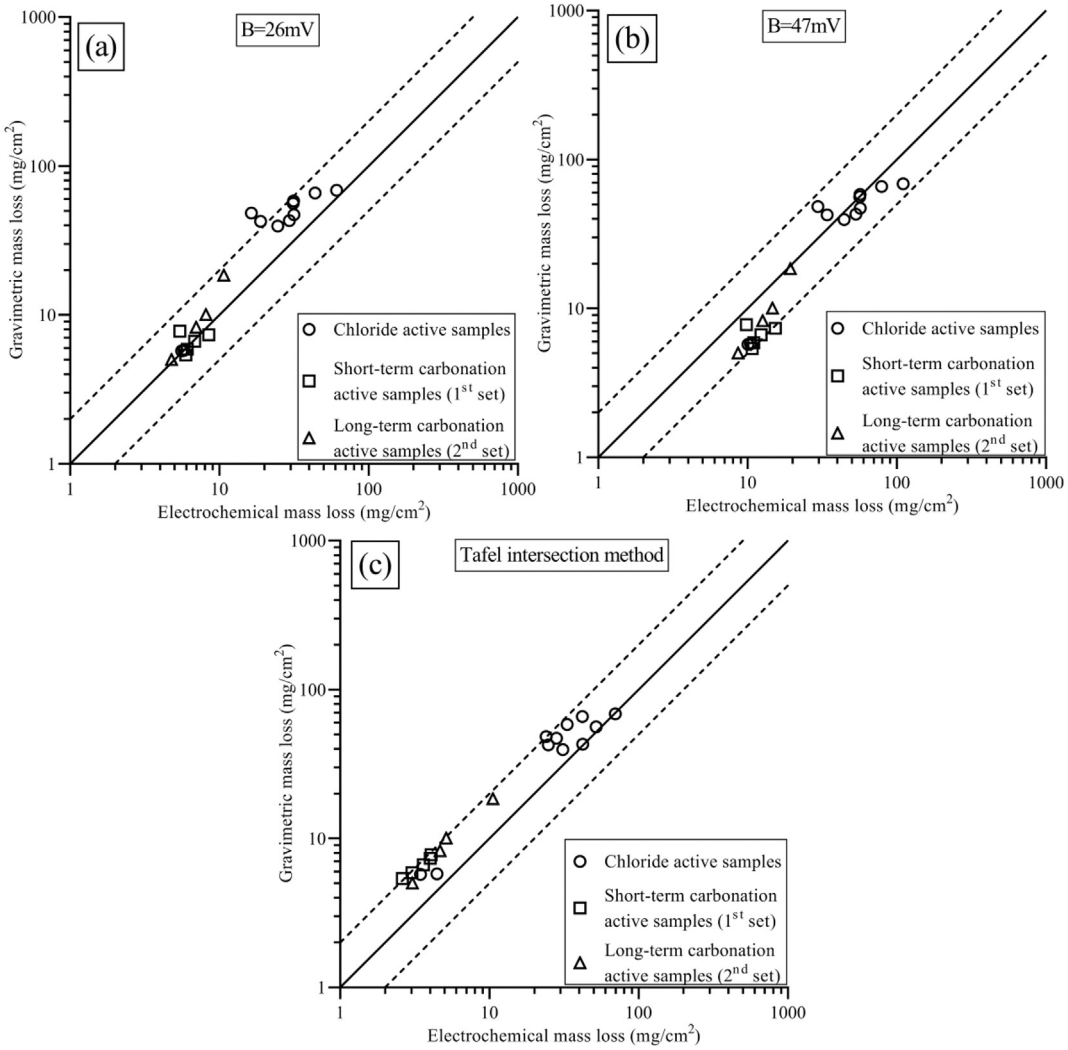

Fig. 11. Comparison between gravimetric mass loss and electrochemical mass loss calculated by using three methods: LPR method with B = 26 mV (a), B = 47 mV (b) and Tafel intersection method (c).

intensity of corrosion current in ampere, t is exposure time in second, n is the electron number transferred per atom (2 for iron) and F is the Faraday constant (96,485.33C/mol). The electrochemical mass losses were determined using the magnitude of corrosion current intensity (I_{corr}) obtained from the Tafel test. In previous studies, bare steel bars or concrete specimens were continually immersed into the testing solution, as a result I_{corr} was constant over time [62,64,70]. The corrosion samples in this study were exposed to repeated wetting/drying cycles throughout the testing period, which leads to a change in intensity of corrosion current from wetting to drying condition. To investigate this effect, moderate overpotential ($\Delta E = \pm 120$ mV) which creates insignificant alteration in corroded system [71] in the end of the wetting submersion was applied to both chloride and carbonated corrosion specimens. Subsequently, a larger range of overpotential ($\Delta E = \pm 250$ mV) was utilized to polarize the reinforcing bars as normal Tafel intersection method. At the end of the 2-weeks drying period, corrosion current intensities were 50% and 75% of the counterpart magnitude in the end of wetting period for chloride and carbonated reinforcement corrosion. Thus, for the integration of I_{corr} over time, only 75% and 87.5% of the corrosion current intensity vs. time total area was taken into account for the calculation of electrochemical mass losses following Faraday's law for chloride and carbonation active corrosion respectively.

Fig. 11(a), (b) and (c) shows the comparison between gravimetric mass loss and electrochemical mass loss by calculating corrosion current intensity using 3 different methods: LPR technique with B = 26 mV, LPR technique with B = 47 mV and Tafel intersection technique. The error factor of 2 in Stern-Geary equation for corrosion current densities was also integrated into Fig. 11 as two dash lines representing upper and lower boundaries of error bands for the mass loss measurements. The corrosion current intensity from LPR method was calculated as the average value from the beginning of the corrosion period until the Tafel test for each steel bar. In Fig. 11(b) and (c), the gravimetric mass loss is comparable to that of electrochemical calculations. All data points were located within two dash lines. In addition, the Tafel intersection method tends to underestimate the electrochemical loss of mass for both chloride and carbonated specimens. Fig. 11(a) shows that using a parameter B of 26 mV seems less accurate. To be specific, 2 out of 20 data points were out of the two error band dash lines. This also reveals that B coefficient of 47 mV is more appropriate for concrete containing flash calcined clay and limestone. Overall, the good agreement between gravimetric and electrochemical mass losses confirms the suitability of the SR selected in Section 3.3 for LC3 concrete specimens to carry out the electrochemical experiments as an inappropriate SR would underestimate or overestimate the corrosion rate as well as electrochemical mass loss.

Due to the combined effects of lower ions concentration (Table 6) and refined porosity in LC3 concrete as previously reported by the authors using similar concrete mixes [19,24], bulk resistivity measured was about 3 times higher than that of reference concrete (Table 3). This can lead to a reduction in ionic current. Moreover, the refined porosity of LC3 concrete may delay oxygen renewal at the steel-concrete interface leading to further reduction of cathodic reactions and ionic currents. This can explain the reduction of the Tafel slopes ($1/\beta_a$ and $1/\beta_c$) observed, justifying the higher "B" constant for LC3 concrete.

The corrosion pattern of active chloride and carbonation-induced reinforcement corrosion bars after 500 days of exposure is showed in Fig. 12. After Tafel extrapolation test, reinforcing bars were removed from the concrete samples and then gently brushed to remove all concrete adhering to the rebar surface. Photos of rebars were taken before and after carrying out the chemical cleaning process. Noticeably, corrosion was not observed on the entire steel surface for both chloride and carbonation corrosion samples. Corrosion products formation was detected only on the steel surface facing the aggressive ions penetration (Cl^- and CO_2) with a concrete cover of 15 mm. Only a uniform corrosion pattern was observed for carbonation-induced reinforcement corrosion whilst mixed uniform and pitting corrosion patterns were noticed in chloride-induced reinforcement corrosion. Similar corrosion patterns were reported in previous studies for conventional OPC concrete [29,72,73]. Corroded rebars of 1st set of carbonation-induced corrosion showed lower corrosion in comparison with 2nd set specimens which is consistent with the electrochemical and mass loss results.

4. Conclusions

The electrochemical behaviours in propagation phase of concrete containing flash calcined clay and limestone as SCM were investigated. Open circuit corrosion potential, polarization resistance, Tafel constants, corrosion current density in both chloride and carbonation-induced reinforcement corrosion was monitored up to 500 days. The gravimetric mass losses were also recorded and compared to the mass losses from electrochemical experiments. The main outcomes derived from this study are summarized as follows:

- A SR of 10 mV/min was selected to run all electrochemical experiments after conducting a set of potentiodynamic cycles from 0.5 mV/min to 1000 mV/min. An appropriate SR generated suitable polarization resistance values resulting in correct corrosion current density (corrosion rate) validated through gravimetric mass loss measurement.
- The evolution of the corrosion potential and the polarization resistance up to 500 days in propagation phase was similar to plain OPC concrete. Corrosion rate classifications for conventional OPC-based concrete were well-agreed with results obtained on LC3 concrete active specimens. For passive specimens, corrosion potentials were in the category of > 90% of having no corrosion activity whilst polarization resistance fell into the low/moderate rate of corrosion. Further studies are recommended to recalibrate the polarization resistance range established for traditional OPC reinforced concrete for passive concrete samples with flash calcined clay and limestone. An exponential correlation could be derived when considering the relationship between corrosion potential and polarization resistance. A remarkably high value of parameter F of 161 from a single-factor analysis of variance (ANOVA) with 50 mV of corrosion potential range indicated the statistical reliability of R_p-E_{corr} relationship, especially for corroded specimens. This relation promotes the capability of corrosion potential to be used as semi-quantitative method for polarization resistance estimation.
- After conducting the Tafel extrapolation method, significant dissimilarities in Tafel constants including β_a, β_c and B were observed between measured results and suggested values for OPC corroded systems. LC3 concrete passive samples displayed a range of B coefficient from 16 mV to 60 mV compared to OPC-based value of 52 mV. For corrosion active samples, insignificant fluctuation of

Table 6
pH and pore solution compositions of cement pastes at 28 days.

Concrete type	pH	Ca (mg/L)	Na (mg/L)	Mg (mg/L)	K (mg/L)	Al (mg/L)	Si (mg/L)	Ti (mg/L)	S (mg/L)
GP cement	13.35	76.5	1831	0	6929	1.26	3.06	0.06	209
LC3	13.15	39.0	1039	0	3937	1.53	4.69	0	73.2

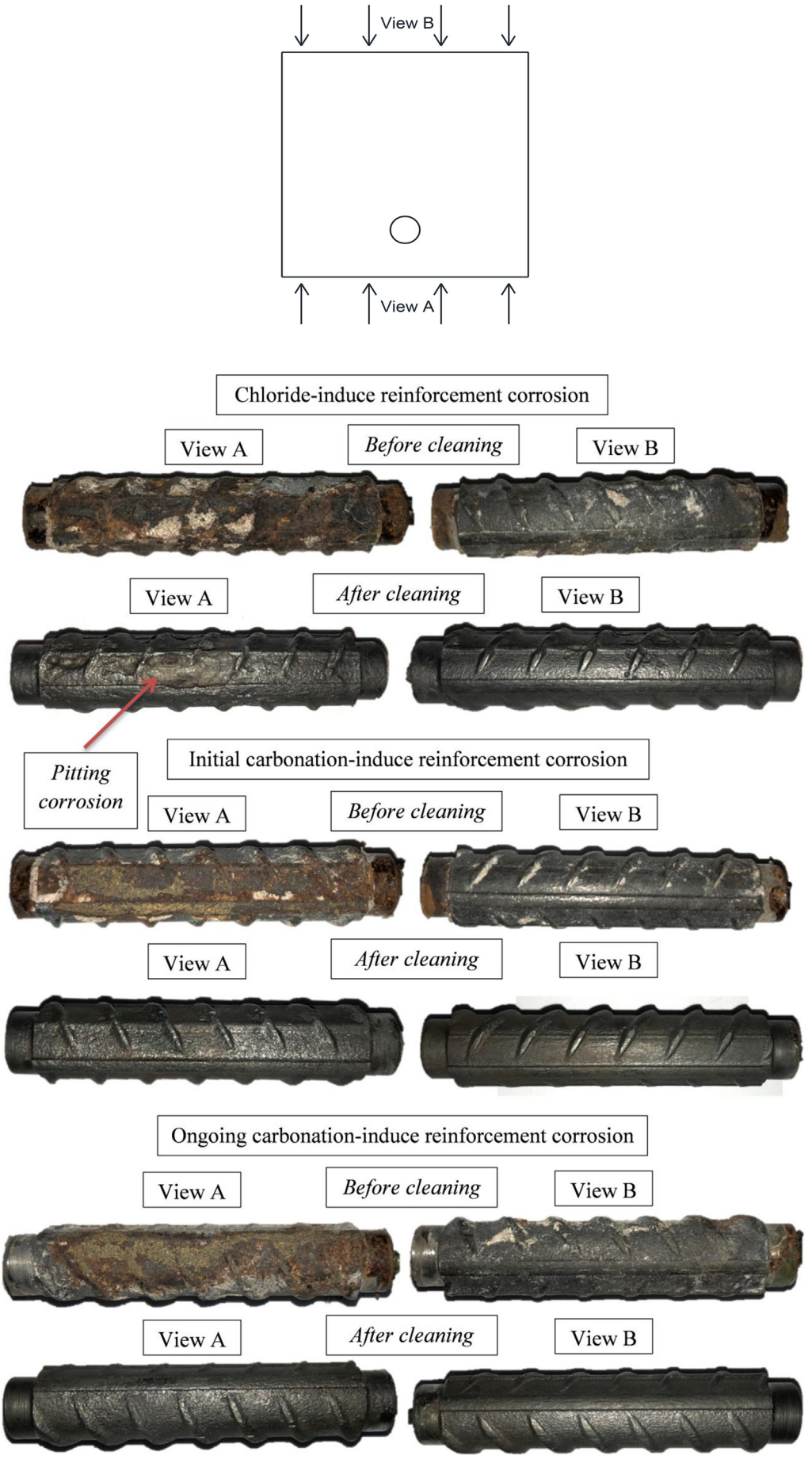

(caption on next page)

Fig. 12. Corrosion pattern of chloride and carbonation-induced reinforcement corrosion.

parameter B was recorded with an average value of 47 mV which is noticeably higher than B = 26 mV in Portland cement concrete. The high electrical resistivity of LC3 concrete specimens induced high anodic and cathodic Tafel slopes leading to a higher B coefficient.

- Good agreement between gravimetric and electrochemical mass loss was observed when considering B value of 47 mV in electrochemical mass loss calculation instead of B = 26 mV. This study allowed to recalibrate the B coefficient in active phase for LC3 concrete. The photos of accumulated corrosion products on reinforcement surfaces taken before conducting gravimetric mass loss measurements were all consistent with electrochemical results.

Overall, performance of reinforced LC3 concrete specimens was comparable to traditional OPC concrete in propagation phase. The conventional electrochemical methods are suitable for concrete containing flash calcined clay and limestone by using recalibrated B = 47 mV in propagation phase.

CRediT authorship contribution statement

Quang Dieu Nguyen:Conceptualization, Methodology, Validation, Investigation, Writing - original draft, Visualization.**Arnaud Castel**:Conceptualization, Methodology, Validation, Writing - review & editing, Supervision, Project administration, Funding acquisition.

Declaration of competing interest

The authors declare that they have no known competing financial interests or personal relationships that could have appeared to influence the work reported in this paper.

Acknowledgements

This research project was funded by the Australian Research Council (ARC Discovery Project DP160104731). The experiments were conducted in Infrastructure Laboratory in the School of Civil and Environmental Engineering at the University of New South Wales. The assistance of the laboratory staff is acknowledged here.

References

[1] U.M. Angst, Challenges and opportunities in corrosion of steel in concrete, Mater. Struct. 51 (2018) 4.
[2] X. Xu, E.E. Bishop, S.M. Kennedy, S.A. Simpson, T.F. Pechacek, Annual healthcare spending attributable to cigarette smoking: an update, Am. J. Prev. Med. 48 (2015) 326–333.
[3] R.A. Hammond, R. Levine, The economic impact of obesity in the United States, Diabetes Metab Syndr Obes 3 (2010) 285–295.
[4] A.B. Smith, R.W. Katz, US billion-dollar weather and climate disasters: data sources, trends, accuracy and biases, Nat. Hazards 67 (2013) 387–410.
[5] G.H. Koch, M.P. Brongers, N.G. Thompson, Y.P. Virmani, J.H. Payer, Corrosion Cost and Preventive Strategies in the United States, (2002).
[6] R.B. Polder, W.H.A. Peelen, W.M.G. Courage, Non-traditional assessment and maintenance methods for aging concrete structures - technical and non-technical issues, Mater. Corros. 63 (2012) 1147–1153.
[7] K. Tuutti, Corrosion of Steel in Concrete, CBI forskning, Cement- och betonginst, (1982), p. 468.
[8] C. Andrade, Propagation of reinforcement corrosion: principles, testing and modelling, Mater. Struct. 52 (2018) 2.
[9] U.M. Angst, M.R. Geiker, A. Michel, C. Gehlen, H. Wong, O.B. Isgor, B. Elsener, C.M. Hansson, R. François, K. Hornbostel, R. Polder, M.C. Alonso, M. Sanchez, M.J. Correia, M. Criado, A. Sagüés, N. Buenfeld, The steel–concrete interface, Mater. Struct. 50 (2017) 143.
[10] A. Favier, C. De Wolf, K. Scrivener, G. Habert, A Sustainable Future for the European Cement and Concrete Industry: Technology Assessment for Full Decarbonisation of the Industry by 2050, ETH Zurich, 2018.
[11] K.L. Scrivener, V.M. John, E.M. Gartner, Eco-efficient cements: potential economically viable solutions for a low-CO2 cement-based materials industry, Cem. Concr. Res. 114 (2018) 2–26.
[12] M. Antoni, J. Rossen, F. Martirena, K. Scrivener, Cement substitution by a combination of metakaolin and limestone, Cem. Concr. Res. 42 (2012) 1579–1589.
[13] G. Medjigbodo, E. Roziere, K. Charrier, L. Izoret, A. Loukili, Hydration, shrinkage, and durability of ternary binders containing Portland cement, limestone filler and metakaolin, Constr. Build. Mater. 183 (2018) 114–126.
[14] A. Tironi, A.N. Scian, E.F. Irassar, Blended cements with limestone filler and kaolinitic calcined clay: filler and pozzolanic effects, J. Mater. Civ. Eng. 29 (2017) 04017116.
[15] R. San Nicolas, M. Cyr, G. Escadeillas, Characteristics and applications of flash metakaolins, Appl. Clay Sci. 83 (2013) 253–262.
[16] M. Claverie, F. Martin, J.P. Tardy, M. Cyr, P. De Parseval, O. Grauby, C. Le Roux, Structural and chemical changes in kaolinite caused by flash calcination: formation of spherical particles, Appl. Clay Sci. 114 (2015) 247–255.
[17] Z.G. Shi, B. Lothenbach, M.R. Geiker, J. Kaufmann, A. Leemann, S. Ferreiro, J. Skibsted, Experimental studies and thermodynamic modeling of the carbonation of Portland cement, metakaolin and limestone mortars, Cem. Concr. Res. 88 (2016) 60–72.
[18] Z.G. Shi, M.R. Geiker, B. Lothenbach, K. De Weerdt, S.F. Garzon, K. Enemark-Rasmussen, J. Skibsted, Friedel's salt profiles from thermogravimetric analysis and thermodynamic modelling of Portland cement-based mortars exposed to sodium chloride solution, Cement Concrete Comp 78 (2017) 73–83.
[19] M.S.H. Khan, Q.D. Nguyen, A. Castel, Performance of limestone calcined clay blended cement-based concrete against carbonation, Adv. Cem. Res. 0 (2019) 1–11.
[20] H. Maraghechi, F. Avet, H. Wong, H. Kamyab, K. Scrivener, Performance of limestone calcined clay cement (LC3) with various kaolinite contents with respect to chloride transport, Mater. Struct. 51 (2018) 125.
[21] K. Scrivener, F. Martirena, S. Bishnoi, S. Maity, Calcined clay limestone cements (LC3), Cem. Concr. Res. 114 (2018) 49–56.
[22] Y. Dhandapani, T. Sakthivel, M. Santhanam, R. Gettu, R.G. Pillai, Mechanical properties and durability performance of concretes with limestone calcined clay cement (LC3), Cem. Concr. Res. 107 (2018) 136–151.
[23] Y. Dhandapani, M. Santhanam, Assessment of pore structure evolution in the limestone calcined clay cementitious system and its implications for performance, Cement Concrete Comp 84 (2017) 36–47.
[24] Q.D. Nguyen, M.S.H. Khan, A. Castel, Engineering properties of limestone calcined clay concrete, J. Adv. Concr. Technol. 16 (2018) 343–357.
[25] R.G. Pillai, R. Gettu, M. Santhanam, S. Rengaraju, Y. Dhandapani, S. Rathnarajan, A.S. Basavaraj, Service life and life cycle assessment of reinforced concrete systems with limestone calcined clay cement (LC3), Cem. Concr. Res. 118 (2019) 111–119.
[26] K. Vance, M. Aguayo, T. Oey, G. Sant, N. Neithalath, Hydration and strength development in ternary portland cement blends containing limestone and fly ash or metakaolin, Cem. Concr. Compos. 39 (2013) 93–103.
[27] E. Badogiannis, S. Tsivilis, Exploitation of poor Greek kaolins: durability of metakaolin concrete, Cement Concrete Comp 31 (2009) 128–133.
[28] S. Krishnan, G.R. Dhoopadahailli, S. Bishnoi, Why low-grade calcined clays are ideal for the production of limestone calcined clay cement (LC3), 3rd International Conference on Calcined Clays for Sustainable Concrete, 2019, pp. 115–120.
[29] R.J. Zhang, A. Castel, R. Francois, Influence of steel-concrete interface defects owing to the top-bar effect on the chloride-induced corrosion of reinforcement, Mag. Concr. Res. 63 (2011) 773–781.
[30] M. Babaee, A. Castel, Chloride-induced corrosion of reinforcement in low-calcium fly ash-based geopolymer concrete, Cem. Concr. Res. 88 (2016) 96–107.
[31] M. Castellote, L. Fernandez, C. Andrade, C. Alonso, Chemical changes and phase analysis of OPC pastes carbonated at different CO2 concentrations, Mater. Struct. 42 (2009) 515–525.
[32] ASTM C39/C39M-18: Standard Test Method for Compressive Strength of Cylindrical Concrete Specimens, ASTM International, West Conshohocken, PA, 2018.
[33] ASTM C469/C469M-14, Standard Test Method for Static Modulus of Elasticity and Poisson's Ratio of Concrete in Compression, ASTM International, West Conshohocken, PA, 2014.
[34] ASTM C496/C496M-17: Standard Test Method for Splitting Tensile Strength of Cylindrical Concrete Specimens, ASTM International, West Conshohocken, PA, 2017.
[35] ASTM C597-16: Standard Test Method for Pulse Velocity Through Concrete, West, Conshohocken, PA, 2016.
[36] A.S.T.M. C642-13, Standard Test Method for Density, Absorption, and Voids in Hardened Concrete, ASTM International, West Conshohocken, PA, 2013.
[37] ASTM C1585-13, Standard Test Method for Measurement of Rate of Absorption of Water by Hydraulic-Cement Concretes, ASTM International, West Conshohocken, PA, 2013.
[38] T. AASHTO, 95-11 "Standard Method of Test for Surface Resistivity Indication of Concrete's Ability to Resist Chloride Ion Penetration", 2011 edition, AASHTO Provisional Standards, 2011.
[39] Q.D. Nguyen, M.S.H. Khan, A. Castel, T. Kim, Durability and microstructure properties of low-carbon concrete incorporating ferronickel slag sand and fly ash, J. Mater. Civ. Eng. 31 (2019) 04019152.
[40] R.S. Barneyback, S. Diamond, Expression and analysis of pore fluids from hardened cement pastes and mortars, Cem. Concr. Res. 11 (1981) 279–285.
[41] ASTM C1152/C1152M-04(2012)e1, Standard Test Method for Acid-soluble Chloride in Mortar and Concrete, ASTM International, West Conshohocken, PA,

2012.
[42] A. Noushini, A. Castel, Performance-based criteria to assess the suitability of geopolymer concrete in marine environments using modified ASTM C1202 and ASTM C1556 methods, Mater. Struct. 51 (2018) 146.
[43] J.A. González, A. Molina, M.L. Escudero, C. Andrade, Errors in the electrochemical evaluation of very small corrosion rates—I. Polarization resistance method applied to corrosion of steel in concrete, Corros. Sci. 25 (1985) 917–930.
[44] M. Stern, A.L. Geaby, Electrochemical polarization, J. Electrochem. Soc. 104 (1957) 56–63.
[45] C. Andrade, C. Alonso, Corrosion rate monitoring in the laboratory and on-site, Constr. Build. Mater. 10 (1996) 315–328.
[46] AS 3600: Concrete Structures Standards Australia, (2018).
[47] A.C. Institute, Building Code Requirements for Structural Concrete (ACI 318-14): Commentary on Building Code Requirements for Structural Concrete (ACI 318R-14): An ACI Report, American Concrete Institute. ACI2014.
[48] BS EN 206, Concrete–specification, Performance, Production and Conformity, BSI, 2014.
[49] A. Noushini, A. Castel, The effect of heat-curing on transport properties of low-calcium fly ash-based geopolymer concrete, Constr. Build. Mater. 112 (2016) 464–477.
[50] J.A. González, A. Molina, M.L. Escudero, C. Andrade, Errors in the electrochemical evaluation of very small corrosion rates—II. Other electrochemical techniques applied to corrosion of steel in concrete, Corros. Sci. 25 (1985) 519–530.
[51] ASTM C876-15, Standard Test Method for Corrosion Potentials of Uncoated Reinforcing Steel in Concrete, ASTM International, West Conshohocken, PA, 2015.
[52] A.M. Aguirre-Guerrero, R. Mejia-de-Gutierrez, M.J.R. Montes-Correia, Corrosion performance of blended concretes exposed to different aggressive environments, Constr. Build. Mater. 121 (2016) 704–716.
[53] C.G. Berrocal, I. Lofgren, K. Lundgren, L.P. Tang, Corrosion initiation in cracked fibre reinforced concrete: influence of crack width, fibre type and loading conditions, Corros. Sci. 98 (2015) 128–139.
[54] I.A. Ammar, S. Riad, Effect of pH on corrosion potentials, J Phys Chem-Us 62 (1958) 150–154.
[55] K.R.G.S.G. Millard, J.S. Gill, Reinforcement Corrosion Assessment Using Linear Polarisation Techniques, Special Publication (1991) 128.
[56] S.G. Millard, D. Law, J.H. Bungey, J. Cairns, Environmental influences on linear polarisation corrosion rate measurement in reinforced concrete, Ndt & E International 34 (2001) 409–417.
[57] R.K. Dhir, M.R. Jones, M.J. Mccarthy, Pulverized-fuel ash concrete-carbonation-induced reinforcement corrosion rates, P I Civil Eng-Str B 94 (1992) 335–342.
[58] G.Y. Koga, B. Albert, R.P. Nogueira, Revisiting the ASTM C876 standard for corrosion of reinforcing steel: on the correlation between corrosion potential and polarization resistance during the curing of different cement mortars, Electrochem. Commun. 94 (2018) 1–4.
[59] O. Kayali, B. Zhu, Corrosion performance of medium-strength and silica fume high-strength reinforced concrete in a chloride solution, Cement Concrete Comp 27 (2005) 117–124.
[60] H.Y. Moon, K.J. Shin, Frost attack resistance and steel bar corrosion of antiwashout underwater concrete containing mineral admixtures, Constr. Build. Mater. 21 (2007) 98–108.
[61] G.L. Song, Theoretical analysis of the measurement of polarisation resistance in reinforced concrete, Cement Concrete Comp 22 (2000) 407–415.
[62] C. Andrade, J.A. Gonzalez, Quantitative measurements of corrosion rate of reinforcing steels embedded in concrete using polarization resistance measurements, Werkst. Korros. 29 (1978) 515–519.
[63] C.E. Locke, A. Siman, Electrochemistry of Reinforcing Steel in Salt-contaminated Concrete, ASTM International, West Conshohocken, PA, 1980.
[64] A. Garces, M.C. Andrade, A. Saez, M.C. Alonso, Corrosion of reinforcing steel in neutral and acid solutions simulating the electrolytic environments in the micropores of concrete in the propagation period, Corros. Sci. 47 (2005) 289–306.
[65] Z.T. Chang, B. Cherry, M. Marosszeky, Polarisation behaviour of steel bar samples in concrete in seawater. Part 2: a polarisation model for corrosion evaluation of steel in concrete, Corros. Sci. 50 (2008) 3078–3086.
[66] A. Michel, M. Otieno, H. Stang, M.R. Geiker, Propagation of steel corrosion in concrete: experimental and numerical investigations, Cement Concrete Comp 70 (2016) 171–182.
[67] K. Hornbostel, C.K. Larsen, M.R. Geiker, Relationship between concrete resistivity and corrosion rate – a literature review, Cem. Concr. Compos. 39 (2013) 60–72.
[68] C. Alonso, C. Andrade, M. Izquierdo, X.R. Novoa, M.C. Perez, Effect of protective oxide scales in the macrogalvanic behaviour of concrete reinforcements, Corros. Sci. 40 (1998) 1379–1389.
[69] J.A. González, C. Andrade, C. Alonso, S. Feliu, Comparison of rates of general corrosion and maximum pitting penetration on concrete embedded steel reinforcement, Cem. Concr. Res. 25 (1995) 257–264.
[70] N. Etteyeb, L. Dhouibi, M. Sanchez, C. Alonso, C. Andrade, E. Triki, Electrochemical study of corrosion inhibition of steel reinforcement in alkaline solutions containing phosphates based components, J. Mater. Sci. 42 (2007) 4721–4730.
[71] Z.T. Chang, B. Cherry, M. Marosszeky, Polarisation behaviour of steel bar samples in concrete in seawater. Part 1: experimental measurement of polarisation curves of steel in concrete, Corros. Sci. 50 (2008) 357–364.
[72] A. Nasser, A. Clement, S. Laurens, A. Castel, Influence of steel-concrete interface condition on galvanic corrosion currents in carbonated concrete, Corros. Sci. 52 (2010) 2878–2890.
[73] R.J. Zhang, A. Castel, R. Francois, Concrete cover cracking with reinforcement corrosion of RC beam during chloride-induced corrosion process, Cem. Concr. Res. 40 (2010) 415–425.
[74] L. Bertolini, B. Elsener, P. Pedeferri, E. Redaelli, R.B. Polder, Corrosion of Steel in Concrete: Prevention, Diagnosis, Repair, John Wiley & Sons, 2013.